Operation of a Microgrid with 100% Inverter-Based Resources

Tamoghna Banerjee, Rabi Shankar Kar, Zhixin Miao, Lingling Fan,
Department of Electrical Engineering
University of South Florida
Tampa, Florida, USA
Emails: {tbanerjee, rskar, zmiao, linglingfan}@usf.edu

***Abstract*—This paper focuses on steady-state operation analysis of a microgrid powered 100% by inverter-based resources (IBRs). In addition to examine the feasibility of such a microgrid, potential operational challenges are identified. A microgrid testbed powered by three IBRs has been built in electromagnetic transient (EMT) simulation environment. Two of the IBRs adopt grid-following control (GFL) with phase-locked-loop (PLL) as the synchronization unit and one IBR adopts grid-forming control (GFM) with frequency-power droop providing synchronization. The paper contributes to testbed building including control setting, formulation of a steady-state load flow analysis problem by translating control logics into equations, and operation challenge identification due to droop parameter setting. The analysis results have been verified by the EMT simulation results.**

***Index Terms*—Microgrid, Inverter-based Resource, Grid-following, Grid-forming, Droop Control, Operation.**

I. Introduction

Modern day utilization of IBR operation has been demonstrated in solar farms, wind farms (Type-3 Induction Generator and Type-4 Permanent magnet synchronous generators), battery energy storage systems (BESS), and HVDC interfaced offshore wind farms [1] [2].

A microgrid may consists of IBRs driven by different sources, e.g., solar or battery. In microgrids, IBR controls play a vital role to operate in either grid-connected or island modes. A key requirement for IBR controls is to provide frequency and voltage support in the island operation mode, while synchronizing to the main grid in the grid-connected mode. In early days, two sets of converter controls are switched upon operation mode change. Such an example is shown in [3] (chapter 9, Fig. 9.15) where a PLL-based GFL control is for the grid-connected mode and a fixed-frequency control is for the island mode. In the bulk power systems, a vast majority of the IBR power plants at the inverter level adopts GFL current vector control. With higher and higher penetrations of IBRs, the grid industry has pushed for IBRs to provide frequency and voltage support [4]. This leads to the many improvements in IBR control design, including many types of grid-forming controls (GFM) [5]. Additionally, the traditional GFL may be enhanced to provide frequency control by adding f-P droop units [5].

The objective of this paper is to examine the feasibility of IBRs based on GFM and enhanced GFL in operation of a microgrid. There will be no need of control structure switching during the transition from grid-connected to islanded modes. To this end, a microgrid testbed powered by three IBRs with different control design structures, has been built in electromagnetic transient (EMT) simulation environment. Two of the IBRs adopt grid-following control (GFL) with phase-locked-loop (PLL) as the synchronization unit and one IBR adopt grid-forming control (GFM) with frequency-power droop provides synchronization.

The paper contributes to IBR-based microgrid EMT testbed building, formulation of a steady-state load flow analysis problem by translating control logics into equations, and operation challenge identification. The analysis results have been verified by the EMT simulation results. Potential operational challenges due to droop parameter setting are identified. Effect of the Q-V droop gain and P-f droop gain of the GFM on stability is particularly emphasized in this investigation.

The paper is organized as follows. Section II introduces the EMT testbed and delves into the details of control logic. The load flow problem formulation is presented in Section III. Section IV presents the simulation results of various events modeled in the system. The effectiveness of IBRs in supporting the grid during voltage dip and load change during autonomous mode is demonstrated through these simulations. The study analyzes and interprets the data obtained, providing valuable insights into the performance of IBRs under different scenarios. Section V concludes the paper by summarizing the key findings of the study.

II. System Topology

The 480-V 60-Hz mcirogrid testbed comprises three IBRs and loads. The three IBRs export a total of 1 MW at the grid-connected mode. A constant DC voltage source of 850 V supplies the DC terminal of IBR, with its AC side connected to an RLC filter. The filter enhances the current and voltage profiles by eliminating high-frequency harmonic components. Given that the controls operates in the dq-frame, the AC three-phase voltage (V_{PCC}) and current (I) measurements, expressed in per-units (pu), undergo an abc/dq conversion process. Subsequently, a power estimator computes the active power (P_{meas}) and reactive power (Q_{meas}) based on the voltage and current measurements in the dq-frame. IBR-1 is capable of producing 0.5 per-unit (pu) of power, while IBR-2 and IBR-3 contribute 0.3 pu and 0.2 pu of power, respectively.

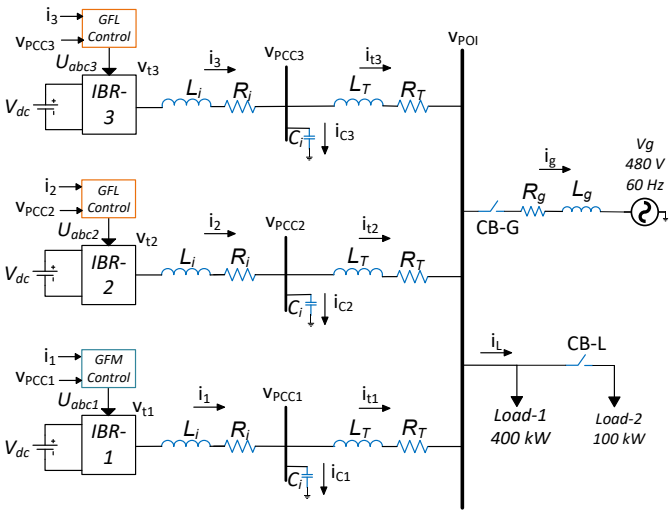

Fig. 1. Schematic diagram of multiple IBRs integrated into a microgrid. Three inverters supplies a total power of 1 MW. The load absorbs 400 kW and the rest of the power goes to the grid.

Each IBR is connected to their own Point of Common Coupling (PCC) bus for measurement and control. All the three PCC buses are connected to a short transmission line and then connected to Point of Intersection (POI) bus. This POI bus interlinks to a load. In order to represent a complex grid a three-phase source of 480 V and 60 Hz is connected to the POI bus and is programmable to receive power from the inverters. IBR-1 is equipped with GFM control, while IBR-2 and IBR-3 are configured with GFL control. The inverters are assumed to have zero inertia and they are simulated as average model to remove the switching dynamics. The system parameters are outlined in Table I. A simulation model of the grid is presented in Fig.1 depicting the microgrid setup with three IBRs. Fig.2 showcases the grid-following and grid-forming control implemented by the inverters.

TABLE I
MAIN PARAMETERS OF THE SYSTEM

Description	Item	Value	Per unit
Rated Power	S_{base}	1 MW	1
Rated Voltage	V_{base}	480 V	1
Nominal Frequency	f	60 Hz	1
Filter Resistance	R_i	0.006912 Ω	0.015
Filter Inductance	X_{Li}	0.0346 Ω	0.15
Filter Capacitance	X_{Ci}	0.217 Ω	20
Transformer Resistance	R_T	0.00046 Ω	0.002
Transformer Inductance	X_{LT}	0.0184 Ω	0.08
Grid Resistance	R_g	0.03456 Ω	0.15
Grid Inductance	X_{Lg}	0.0576 Ω	0.25
Load	P_{L1}	400 kW	0.4
GFM d-axis PI	$[K_{\text{pV}_\text{d}}, K_{\text{iV}_\text{d}}]$	-	0.6, 60
GFM q-axis PI	$[K_{\text{pV}_\text{q}}, K_{\text{iV}_\text{q}}]$	-	0.4, 40
GFL d-axis PI	$[K_{\text{pP}}, K_{\text{iP}}]$	-	0.25, 25
GFL q-axis PI	$[K_{\text{pQ}}, K_{\text{iQ}}]$	-	0.25, 25
Current Control	$[K_{\text{pI}}, K_{\text{iI}}]$	-	0.5, 3
Droop Control	$[m, n]$	-	5%, 0.5
V, Q orders in droop			1, 0
PLL	$[K_{p\text{PLL}}, K_{i\text{PLL}}]$	-	60, 1400

A. Grid-Forming Control

The GFM converter, depicted in Figure 2(a), operates as a voltage source at a frequency of 60 Hz while employing an power droop control mechanism. The $P-f$ droop control, also known as power synchronization; regulates the frequency and angle (θ), while the $Q-V$ droop control sets the d-frame reference voltage ($V_{\text{d,ref}}$). In the presence of load changes, the $P-f$ droop control adjusts the power set point to accommodate any resulting frequency deviations [6] [7]. The droop for GFM is defined in (1)-(2) and is only applicable for IBR-1.

$$\omega_{\text{pu}} = 1 + m(P^* - P) \tag{1}$$

$$V_{\text{PCC,d}} = 1 + n(Q^* - Q) \tag{2}$$

In the outer-loop of GFM control, the measured V_{dq} values are compared to their corresponding reference values, $V_{\text{dq,ref}}$, and are then processed through a proportional-integral (PI) controller to generate the desired $i_{\text{dq,ref}}$ signal. The reference signal $V_{\text{d,ref}}$ in the outer loop is determined by the $Q-V$ droop control, while $V_{\text{q,ref}}$ remains fixed at zero. Moving to the inner-loop control, the $i_{\text{dq,ref}}$ signal is compared to the measured $I_{\text{dq,meas}}$ and is further processed through another PI controller to generate the modulation signal for the Voltage Source Converter (VSC). A feed-forward loop is incorporated to decouple the current dynamics. To ensure stability and prevent excessive deviations, current and voltage limiters are implemented within the PI controllers [8] [9].

B. Grid-Following Control

The GFL control, depicted in Figure 2(b), is employed in the two remaining IBRs to regulate real and reactive power to the grid. f-P and V-Q droop are added to regulate the reference values P_{ref} and Q_{ref} respectively. The droop control for GFL is defined in (3)-(4) and used in IBR-2 and IBR-3.

$$P_{\text{ref}} = P^* + \frac{1}{m}(1 - \omega_{\text{pu}}) \tag{3}$$

$$Q_{\text{ref}} = Q^* + \frac{1}{n}(1 - V_{\text{PCC,d}}) \tag{4}$$

In the outer-loop control, the measured active and reactive power, P_{meas} and Q_{meas}, respectively, are compared to their respective reference values, P_{ref} and Q_{ref}, and then processed by a proportional-integral (PI) controller to generate the reference current in the $dq-$frame, denoted as $i_{\text{dq,ref}}$. The inner-loop control compares $i_{\text{dq,ref}}$ with the measured dq-frame current, $i_{\text{dq,meas}}$, and passes the result through another PI controller to generate the modulation signal for the inverter bridge.

The PLL is a very important component for GFL control. The PLL provides the synchronization angle θ for the GFL control generated dq voltage command for the converter to be converted to the abc-frame signals. The PLL enforces the PCC voltage space vector's projection on its dq-frame to be aligned to the d-axis. Therefore, the q-axis component of the PCC voltage is enforced to be 0 at steady state.

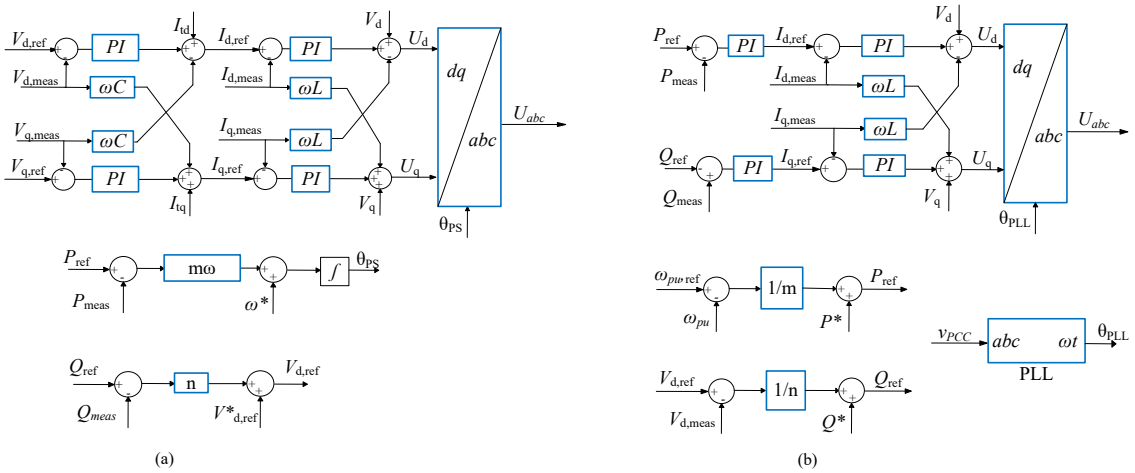

Fig. 2. Inverter Control with their respective droops. (a) GFM. (b) GFL.

Through PQ regulation, the GFL IBRs can manage the power support to the grid. In the grid-connected mode, the IBRs can export power according to the power reference since the operation frequency is 60 Hz at steady state. At grid-connected mode, the GFM also operates at 60 Hz. Hence, its exporting power also matches its power reference. The V-Q and Q-V droops have its voltage and reactive power orders set at 1 pu and 0 pu. The gain of V to Q is set 0.5 while the gain of Q to V is set at 2. Therefore, if the reactive power exporting level is 0 pu, the PCC bus voltage of the IBR is 1 pu. If the reactive power exporting level is -0.1 pu, the IBR's voltage is 1.05 pu.

In the islandedmode, the frequency of the system will depend on the power references and the load power. The voltage of the PCC bus will depend on the V-Q droop parameters, VQ references, and the load reactive power consumption.

III. Steady-State Analysis

We use MATLAB toolbox YALMIP to carry out load flow analysis. YALMIP is designed for the resolution of optimization quandaries, notably those founded on linear matrix inequalities (LMIs) and semidefinite programming (SDP) [6]. It can be used for nonlinear equation calculation by treating the set of equations as equality constraints of an optimization problem. For the islanded mode, there are following unknowns:

$$\text{Unknowns: } V_{\text{PCCi}}, V_{ti}, I_i, I_{ti}, S_i, V_{\text{POI}}, \omega_{\text{pu}}$$

where $i = 1, 2, 3$ notates the IBRs. There are a total of 17 unknowns in the real domain. These include the converter voltage and current, PCC voltage, line current, POI voltage, the complex power generated from the inverter, and finally the frequency of the system. The voltage, current and power relationship is based on circuit analysis according to the circuit in Fig. 1.

$$S_i = V_{\text{PCCi}} \cdot I_i^* \tag{5}$$

$$V_{\text{PCCi}} = V_{ti} - I_i(R_i + jX_{\text{Li}}) \tag{6}$$

$$I_{ti} = I_i - \frac{V_{\text{PCC}}}{-jX_{\text{Ci}}} \tag{7}$$

$$V_{\text{POI}} = V_{\text{PCCi}} - I_{ti}(R_T + jX_T) \tag{8}$$

$$V_{\text{POI}} = R_{\text{Load}} \cdot \sum_{i=1}^{3} I_{ti} \tag{9}$$

Note that in the circuit calculation, a nominal frequency is assumed since we assume that the operating frequency is very close to 60 Hz.

(5) takes care of the complex power generated by the inverter. Using KVL we can define the parameters of V_{PCC} and V_{POI} in (6)-(8). While (7) is the application of KVL to determine the line current I_t from the inverter current I. Each PCC branch produces a current i_{tk} which reaches the POI bus.

(1)-(4) are also incorporated to add the droop dynamics into the load flow calculation. Ultimately, the optimization solver finds solutions that satisfy the web of equations.

IV. Simulation Results

The EMT simulation testbed was built in MATLAB/Simscape specialized power systems. Simulation starts with all the IBRs connected and the main grid is connected to the microgrid. Two test cases are performed to examine dynamic responses of the microgrid. The first one is a voltage dip of main grid voltage source during grid-connected mode. The voltage dip remains for a short period of time and then resumes to normal voltage. The second study case is to switch from the grid-connected mode to autonomous mode. All IBRs are supplying the load based on their control settings.

In the initial stage of Case 1, the three IBRs produce a total power of 1 MW, and the loads are consuming 400 kW. The rest 600 kW is supplied back to the grid.

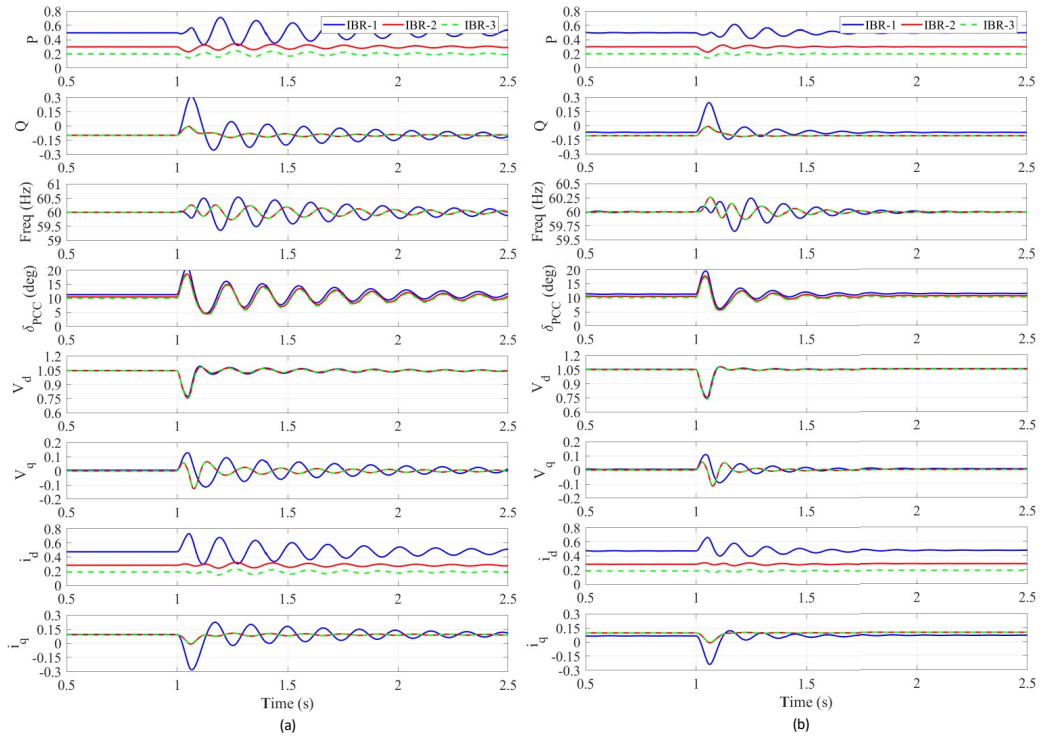

Fig. 3. The IBR dynamic performance upon grid voltage dip. The voltage reduced from 1 pu to 0.5 pu for 3 cycles (from 1 to 1.05 seconds). (a) Q-V droop gain n is 0.5. (b) Q-V droop gain n is 0.8.

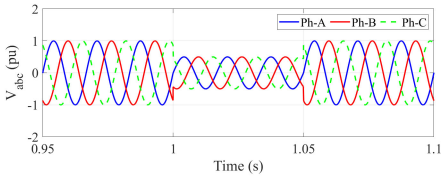

Fig. 4. Voltage and Current profile of grid source during grid voltage dip. The voltage reduced from 1 pu to 0.5 pu for 3 cycles (from 1 to 1.05 seconds).

A. Voltage Dip Dynamics

A grid voltage dip is applied for a short period of 3 cycles or 0.05 s (1s -1.05 s). The magnitude of the voltage drops from 1 pu to 0.5 pu as shown in Fig. 4. This dynamic responses are shown in Fig. 3 (a). The system is subject to a slowly damped oscillation at 6 Hz.

Fig. 3 (a)'s plots of angles and voltages show that the three IBRs behave very similarly. On the other hand, it is seen that in the frequency, real and reactive power measurements, IBR-1 (GFM) and the other two IBRs (GFL) behave very differently. The GFM based IBR-1 provides more reactive power at the instant of voltage dip. This difference is caused by the difference in control.

IBR-1's real power and reactive power have much severe oscillations compared to other two. Since the grid's impedance is relatively large, this type of oscillations can be viewed as a type of weak grid oscillations [10], [11]. Therefore, to mitigate the oscillations, IBR-1's control parameters are tuned. Observing the voltage-reactive power droop control equation in (2), it can be seen that n's effect is to reduce the effect of the grid reactance (recall that $\Delta V \approx X_g \Delta Q$ for a purely inductive grid [12]). Therefore, a small n is equivalent to a weaker grid. Increasing n is equivalent to increase grid strength by reducing the voltage sensitivity towards reactive power injection. Hence n may be increased. Fig. 3(b) shows the dynamic performance of the IBRs when IBR-1's Q-V droop gain n increases from 0.5 to 0.8. It can be seen that the oscillations are quickly damped out.

B. Autonomous Mode

At 1 s, the grid is intentionally disconnected from the microgrid. The disconnection, facilitated by a three-phase breaker (CB-G), introduces some switching dynamics in the system, leading to noticeable spikes. Fig. 5 illustrates the three IBRs dynamic performance on powers, frequency, voltages and currents. All IBRs participate in voltage and frequency support. IBR-1's response is much faster compared to the other two IBRs. The power of all three IBRs experiences a reduction in power supply ($\Delta P_i = -0.2$ pu) since the load consumes only 400 kW. Due to the 5% droop set in each IBR, this reduction of power leads to increase in frequency from 60 to 60.60 Hz:

$$\Delta f = -5\% \cdot \Delta P_i = -5\% \times (-0.2) \text{ pu} = 0.06 \text{ Hz}.$$

At 2 s, there is an increase in the load power consumption by 0.1 pu when the load circuit breaker (CB-L) is turned on.

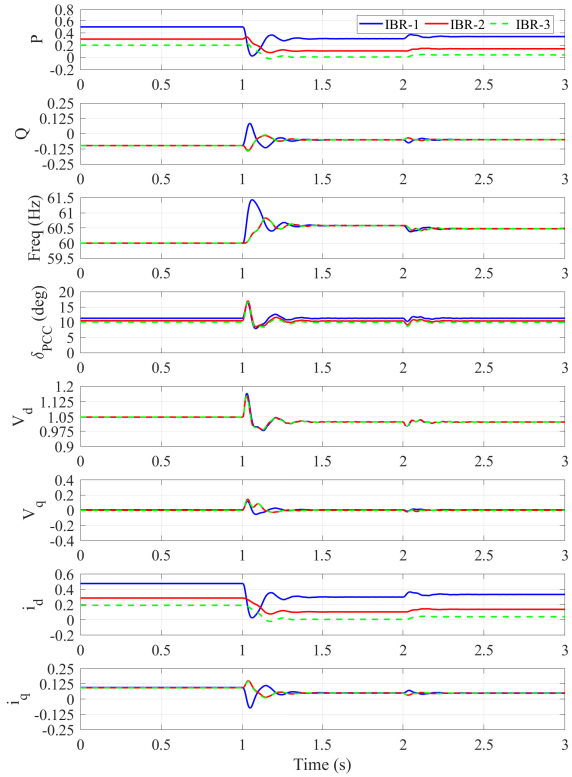

Fig. 5. Autonomous mode operation with all inverters at 5% droop. At 1 s, the grid source is disconnected, and at 2 s, the load is increased by 0.1 pu.

Consequently, the power output of the three IBRs increase slightly ($\Delta P = 0.033$ pu), and the $P - f$ droop effect causes the system frequency to decrease to 60.49 Hz. These values of power and frequency verifies the load flow analysis results.

In an isolated incident, the IBR-1 droop coefficient is changed to examine the P-f droop parameter's influence. Fig. 6 shows the impact of different droop coefficients in GFM control only. It can be seen that a smaller P-f droop gain makes frequency deviation smaller upon power change. On the other hand, this small droop gain introduces 16-Hz ripples in real and reactive power measurements. It appears that the ripples are more significant in IBR-2 and IBR-3's frequency measurements, implicating that PLLs of the GFL control may play a role in making 16-Hz more severe. Further mechanism analysis is necessary.

V. Conclusion

This research conducts a comprehensive operational assessment of a microgrid powered by grid-forming and grid-following IBRs. In both control structures, P-f and Q-V droop control has been deployed to provide frequency and voltage support. A testbed has been built in this research for detailed EMT simulation analysis. Furthermore, a load flow problem is formulated for steady-state analysis. The analysis results have been verified by the EMT simulation results. Two operational challenges have been identified, namely, a small V-Q droop

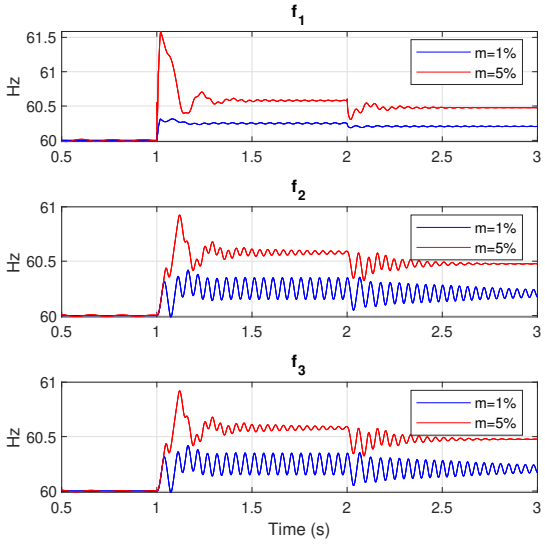

Fig. 6. Responses of all inverters during autonomous mode of operation with GFM inverter when m is 1% (blue line) or 5% (red line). At 1 s, the grid source is disconnected, and at 2 second mark, the load is increased by 0.1 pu.

gain in the GFM may introduce weak grid oscillations at 6 Hz and a small P-f droop gain may introduce 16-Hz ripples in real and reactive power measurements in autonomous mode.

References

[1] L. Fan, Z. Miao, D. Ramasubramanian, and H. Ding, "Operational challenges of solar pv plus storage power plants and modeling recommendations," *IEEE Open Access Journal of Power and Energy*, vol. 10, pp. 477–489, 2023.

[2] A. Aljumah, Z. Miao, and L. Fan, "Stability analysis of grid forming converter using 3-by-3 admittance measurements," *IEEE PESGM*, 2022.

[3] A. Yazdani and R. Iravani, *Voltage-sourced converters in power systems: modeling, control, and applications*. John Wiley & Sons, 2010.

[4] NERC, "White paper: Grid forming functional specifications for bps-connected battery energy storage systems," 2023.

[5] L. Fan and Z. Miao, *Modeling and stability analysis of inverter-based resources*. CRC Press, 2023.

[6] J. Efberg, "Yalmip : A toolbox for modeling and optimization in matlab," *2004 IEEE International Symposium on Computer Aided Control Systems Design*, Taipei, Taiwan, September 24,2004.

[7] O. Tremblay, L.-A. Dessaint, and A.-I. Dekkiche, "A generic battery model for the dynamic simulation of hybrid electric vehicles," *Vehicle Power and Propulsion Conference*, vol. 284-289, 2007.

[8] B. Badrzadeh, S. D. Graff, P. Hinkel, L. Kothalawala, R. Liu, S. Mcguiness, C. Noronha, D. Ramasubramanian, and V. Singhvi, "Tools an techniques for system restoration," *CIGRE Sience and Engineering, Febuary 20*, 2021.

[9] M. A. et al., "Power system restoration - a task force report," *IEEE Transactions on Power Systems*, vol. 2, pp. 271–277, 1987.

[10] Y. Cheng, L. Fan, J. Rose, S.-H. Huang, J. Schmall, X. Wang, X. Xie, J. Shair, J. R. Ramamurthy, N. Modi *et al.*, "Real-world subsynchronous oscillation events in power grids with high penetrations of inverter-based resources," *IEEE Transactions on Power Systems*, vol. 38, no. 1, pp. 316–330, 2023.

[11] L. Fan, "Modeling type-4 wind in weak grids," *IEEE Transactions on Sustainable Energy*, vol. 10, no. 2, pp. 853–864, 2019.

[12] L. Fan, Z. Miao, D. Piper, D. Ramasubramanian, L. Zhu, and P. Mitra, "Analysis of 0.1-hz var oscillations in solar photovoltaic power plants," *IEEE Transactions on Sustainable Energy*, vol. 14, no. 1, pp. 734–737, 2023.